IEEE Access
Multidisciplinary | Rapid Review | Open Access Journal

Received November 19, 2019, accepted December 5, 2019, date of publication December 10, 2019,
date of current version December 23, 2019.

*Digital Object Identifier 10.1109/ACCESS.2019.2958880*

# Train Impedance Reshaping Method for Suppressing Harmonic Resonance Caused by Various Harmonic Sources in Trains-Network Systems With Auxiliary Converter of Electrical Locomotive

**SHIHUI LIU[1], (Student Member, IEEE), FEI LIN[1], (Member, IEEE), XIAOCHUN FANG[1], (Member, IEEE), ZHONGPING YANG[1], (Member, IEEE), AND ZHIWEI ZHANG[2], (Member, IEEE)**

[1]School of Electrical Engineering, Beijing Jiaotong University, Beijing 100044, China
[2]Department of Electrical and Computer Engineering, The Ohio State University, Columbus, OH 43210, USA

Corresponding authors: Shihui Liu (14121430@bjtu.edu.cn) and Xiaochun Fang (xcfang@bjtu.edu.cn)

This work was supported by the Fundamental Research Funds for the Central Universities of China under Grant 2018YJS158.

**ABSTRACT** With the development of electrified railway, harmonic resonance accidents occur from time to time. Based on the mechanism of resonance, a harmonic resonance suppression radical method by impedance reshaping is proposed. Thus, the equivalent impedance of the train position is significantly reduced. Compared with the traditional method of improving harmonic current, this method of impedance reshaping can not only suppress the resonance caused by its own harmonic, but also suppress the resonance caused by other trains or other unknown harmonic sources. Harmonic impedance of the train in the resonant frequency is reshaped by detecting the resonance voltage and controlling the auxiliary converter harmonic current. The resonance identification and parameter settings of the impedance reshaping control are also discussed. The proposed harmonic resonance suppression strategy is fully tested with an auxiliary converter control in a simulation trains-network system model. The performance of the proposed strategy is further evaluated on the experimental platform. Both the results verify the effectiveness and feasibility of the proposed strategy. The application of SiC devices makes it effective to suppress the resonance of thousands of hertz. The experiment was validated in two cases. One is the resonance caused by the harmonic current of the train itself. The second is the resonance caused by the harmonic current of trains in other locations. In both cases, the train using impedance reshaping method can ensure that the resonance of its position is effectively suppressed.

**INDEX TERMS** Active filters, AC-DC power converters, harmonic analysis, resonance, railway accidents, railway safety, traction power supplies.

## I. INTRODUCTION

With the large-scale use of electrified trains including high-speed trains, harmonic resonance is becoming more and more prominent in traction networks. When harmonics of trains match the peak impedance of the traction network, harmonic resonance may occur with amplified harmonic voltage from hundreds to thousands of hertz. This not only affects the normal operation of the train, also results in security problems. Accidents such as tripping, lightning arrester burnout and train outage often occur. Even other trains on the same power arm are affected. This kind of harmonic resonance phenomenon was first reported in the field of electrified railway in Switzerland, harmonic current caused multiple train protection device action, train outage [1]. Since that time multiple harmonic resonance accidents have also occurred

The associate editor coordinating the review of this manuscript and approving it for publication was Yuh-Shyan Hwang.

in other parts of Europe, Japan, South Korea and China [2]. With the rapid development of high-speed railways in China, harmonic resonance accidents began to occur in 2007. Hundreds to thousands of Hertz resonance accidents occur on different lines, resulting in the burnout of equipment and traction power loss.

The research of harmonic resonance in the trains-network system mainly focuses on the modelling and analysis of trains and traction networks, as well as the reappearance of harmonic resonance phenomenon and mechanism analysis [3]–[6]. The model of the train is often simplified as a four-quadrant converter (4QC). It is usually represented by a constant current model for harmonic studies [7], [8]. The impedance of the 4QC will affect the traction network analysis [9]. A harmonic current from the train and the impedance of the traction network form a resonant circuit, causing the train terminal voltage current amplitude to increase significantly. In China's electrified railways, the all-parallel AT-fed catenary system is the most commonly used traction network structure. The traction network model mainly contains the equivalent circuit model, generalized symmetrical component model, and chain-circuit model [10].

In the field of electrified railway, the most common method to suppress resonance is to minimize the harmonics or change the frequency of the harmonic current [11]–[13]. In practical application, adopting passive filters is a common method to reduce harmonic current. The active power filter is also used for resonance suppression [14]. Compared with a passive filter, an active power filter has faster response speed and compensation characteristics of a dynamic harmonic suppression device. Most active power filters use the PWM converter as the main circuit [15]. At present, the most studied resonance situation is that the harmonic of the train itself matches the harmonic impedance frequency of its location. However, not all resonance accidents are caused by harmonics of the train in the accident point. In fact, other harmonic sources, mainly other trains, will also generate harmonics, and these harmonics will propagate over the traction network. Reducing harmonics is effective for partial resonances, but not for all resonances. When the train runs to a position where the characteristic impedance of the corresponding frequency is very large, the harmonics from other sources will also resonate in this position. Our goal is to find an effective method for all resonances by changing the impedance at the location of the train.

In the field of power system, there are some studies on changing the fixed position impedance. Active damping mainly uses the control algorithm to simulate the system damping resistance [16]–[18], and a shunt active damping device is parallel to the public point [19]–[22]. The resistive active filter (R-APF) uses a high pass filter to extract the harmonic component, then multiplies the harmonic component by a gain to simulate the damping resistor. It is often parallel to the end of the line. R-APF can be equivalent to a damping resistance at the harmonic frequency, so that the harmonic resonance can be suppressed [23]. R-APF has been applied to the power grid system effectively [24]. R-APF needs extra hardware facilities, such as an extra converter. The installation position of the device is fixed. Some researchers have addressed the influence of the positions of the different active filters when there are many active filters installed in the system [25], [26].

Compared with the power system, the railway system has some characteristics that cannot be ignored. The train needs to run continuously, and the position of the train changes constantly, which also means that the harmonic source is moving. The impedance of the traction network at the location of the train is also changing with time. Owing to the complex impedance characteristics of traction networks, harmonic impedances in some specific frequencies may reach high value. Different trains also interact with each other. It is hard for traditional methods to adapt to the situation that the train position and circuit topology are constantly changing in electrified railway.

We propose an effective way to meet changes of train position, its equivalent impedance, harmonic content and harmonic frequency in railway system. Considering that the train itself has auxiliary converters, integrating the impedance reshaping control into the auxiliary converter of the train is a feasible method. The proposed train impedance reshaping method can not only suppress the resonance caused by its own harmonic, but also suppress the resonance caused by other trains or other unknown harmonic sources. It can adapt to the change of system topology and harmonic current caused by the change of position and working condition. By keeping each train free from resonance, it ensures the normal operation of the whole system.

The second section introduces the trains-network system and harmonic resonance mechanism. In the third section, the control of the harmonic resonance suppression function for the auxiliary four quadrant converter is discussed, the influence of control parameters is analyzed, and the suppression strategy of impedance reshaping control is given. The fourth part details the simulation of the concrete parameter and proves the correctness of theory analysis. In the fifth part, the experimental platform and experimental results on it are introduced. Finally, the sixth part is a summary of the full text.

## II. TRAINS-NETWORK SYSTEM HARMONIC RESONANCE AND SUPPRESSION ANALYSIS

### A. INTRODUCTION OF THE TRAINS-NETWORK SYSTEM

A schematic diagram of trains-network system is shown in Fig. 1. T represents contact lines; R represents rails and F represents positive feeders. The whole traction network can be equivalent to an RLC circuit. The railway traction power supply networks and the rectifier side of the traction converter and auxiliary converter of the train all use single-phase electricity.

The primary side of the main transformer of the train is the traction network side. On this side, the fundamental

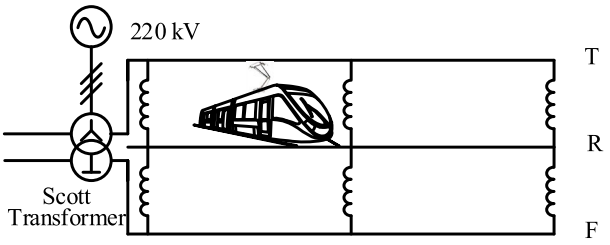


**FIGURE 1.** Schematic diagram of trains-network system.

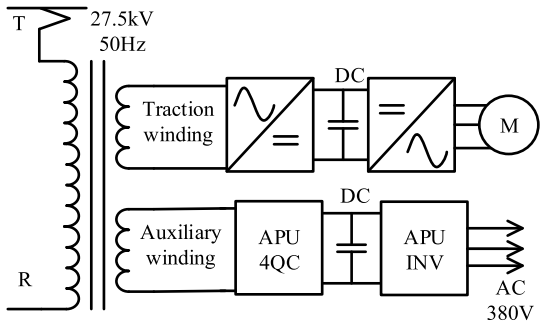


**FIGURE 2.** Schematic diagram of train main circuit.

component of the supply voltage corresponds to 27.5kV. In general, it is necessary to have a separate converter to achieve the function of compensating current. In addition to the traction winding, there is also a separate auxiliary winding for the auxiliary converter in some trains as shown in Fig. 2.

Harmonics of the traction drive system are mainly in the following categories: harmonics around the integral multiple of switching frequency, medium frequency harmonics, and low frequency harmonics such as $3^{th}$, $5^{th}$ and $7^{th}$ harmonic. For the harmonic resonance of trains, the generation of harmonics is mainly related to the switching frequency of PWM. The frequency of harmonic resonance is usually in the frequency range from several hundred to several thousand hertz. For relatively high harmonic frequencies, a higher switching frequency is required to generate a corresponding instruction. The application of SiC devices makes it effective and possible to suppress higher frequency resonance in this paper.

### B. HARMONIC RESONANCE MECHANISM

Fig. 3 is the schematic diagram of the characteristic impedance of the power supply arm of the traction network at different frequencies. The abscissa represents the frequency, and the ordinate represents the impedance of the point at this frequency. At some specific frequencies, the corresponding impedance value has a peak value which is much higher than the impedance value at other frequencies. The frequency corresponding to the peak value is the characteristic frequency of the point of the power supply arm, and the impedance corresponding to this point is the characteristic impedance. In general, the characteristic frequencies of the same power supply arm are several fixed frequencies, and the characteristic impedance corresponding to each frequency varies with the position.

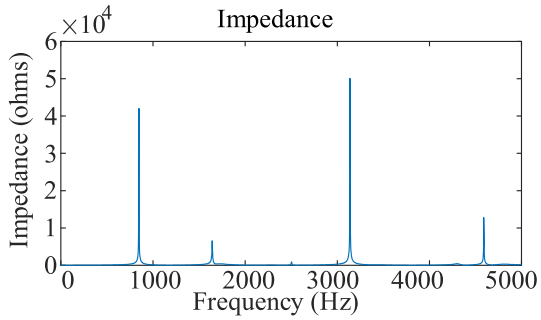


**FIGURE 3.** Schematic diagram of characteristic impedance of power supply arm of the traction network under different frequencies.

The harmonics generated by the train converters can be transmitted to the traction network. When the frequency of the harmonics of the train corresponds to the frequency of the characteristic impedance of the traction network, the harmonic resonance occurs and produces overvoltage. Whether the resonance is caused by the harmonic of the controlled train or other trains in the same traction power supply system, the resonance can be calculated as follows. The product of the harmonic current amplitude and the amplitude of the impedance determines the amplitude of the resonant voltage, while the impedance parameters determine the resonance frequency. The harmonic voltage or current will be mainly distributed on the characteristic frequency, thus the focus of the resonance suppression is to eliminate the voltage and current content of the characteristic harmonic resonance frequency. The resonance can be suppressed by reducing the amplitude of the impedance.

### C. HARMONIC RESONANCE SUPPRESSION METHOD

As shown in Fig. 4 (a), there are two trains on the same power supply section. The left train with the main circuit diagram shows that this train is controllable, while the train showing the appearance on the right is uncontrollable. If harmonic resonance occurs on the left train, there are two possible reasons for this. One is that the harmonic current of the left train matches the frequency of the characteristic impedance of the traction network at the position of the train and produces resonance. Even if the train's own harmonics do not exceed the standard, provided that the characteristic impedance is substantially large, the resonance can still occur. In the other case, harmonics of other trains on the traction network, such as the right train, are injected into the traction network. Harmonics are propagated to the position of a controlled train, which match the impedance of the site and produces resonance. In this case, the harmonic source in other positions of the traction network is not controllable. The method adopted in this paper is applicable to both cases discussed above.

According to the resonance mechanism, to suppress the harmonic resonance, it is necessary to reduce the harmonic impedance. The impedance reshaping control can be considered as paralleling additional virtual impedance at the connection point to reduce the equivalent impedance, to obtain the effect of resonance suppression.

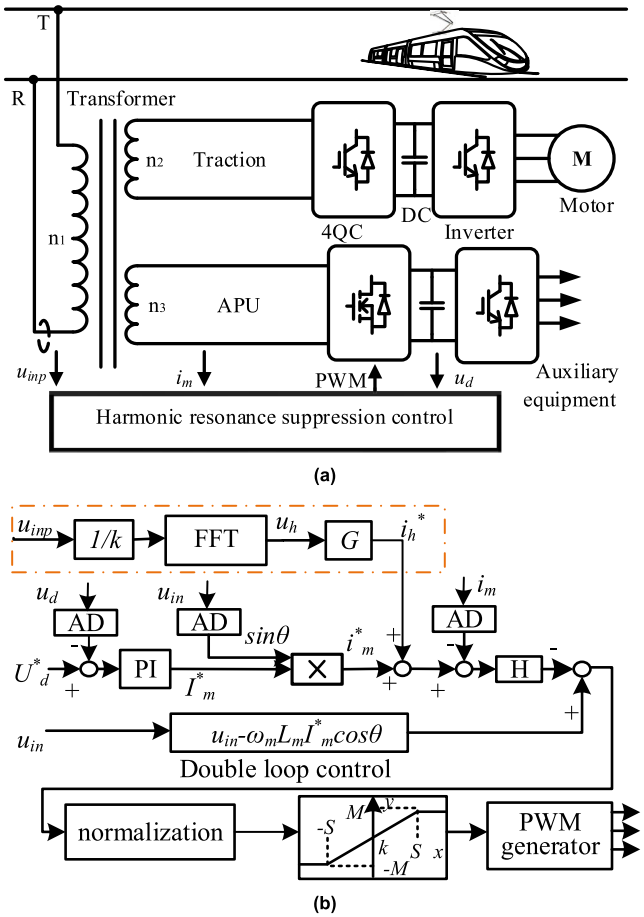


**FIGURE 4.** Control block diagram of harmonic resonance suppression (a) System block diagram, (b) APU Schematic diagram of harmonic resonance suppression.

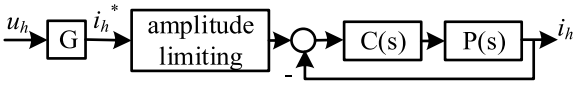


**FIGURE 5.** Simplified control block diagram of harmonic instruction.

The original control strategy [27] of four-quadrant converter is the double-loop control. $U_d{}^*$ is the DC-link voltage command, and $U_d$ represents the DC output voltage sampled value. The current command ($i_m{}^*$) amplitude is derived from the PI controller output, while the current command phase is from the input voltage source sampled value.

The ratio of the primary winding, $n_1$, to the auxiliary winding, $n_3$, of the main transformer is $k$.

$$k = n_1 / n_3 \tag{1}$$

The impedance reshaping control is added to the original control strategy as shown in Fig. 4 (b). The theta parameter is obtained through a PLL circuit. Corresponding to the harmonic source and characteristic impedance peak in different positions, we must detect the primary voltage of the transformer [28]. The voltage of the primary side, $u_{inp}$, is converted by the proportional $k$ and harmonic voltage, $u_h$, is obtained by FFT. Moving window of FFT analysis contains 800 sampling points [29]. The harmonic current instruction, $i_h{}^*$, is added to the original auxiliary converter current instruction.

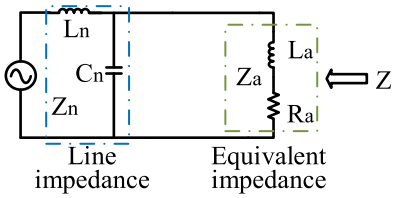


**FIGURE 6.** The parallel equivalent impedance changes the impedance.

## III. CONTROL OF HARMONIC RESONANCE SUPPRESSION FUNCTION FOR AUXILIARY CONVERTER

### A. SUPPRESSION ANALYSIS OF IMPEDANCE RESHAPING CONTROL FOR AUXILIARY CONVERTER

As shown in Fig. 5, the harmonic current command value $i_h{}^*$ is obtained after the voltage value $u_h$ of the detected harmonic resonance frequency is converted to $G$.

$$i_h^* = G \times u_h \tag{2}$$

$$C(s) = H \tag{3}$$

$$P(s) = 1/(sL_m + R_m) \tag{4}$$

Among them, $L_m$ is the auxiliary converter AC side inductance which can be measured, $R_m$ is the auxiliary converter stray resistance which is very small and typically negligible. The $C(s)$ is the control link. The proportional control is applied in this paper, and the proportionality factor is $H$. $P(s)$ is the controlled object of the current loop, which corresponds to the main circuit of the converter. The harmonic current $i_h$ is the harmonic component of the converter AC current $i_m$. The transfer function of closed current control loop is calculated as follows:

$$\frac{i_h}{i_h{}^*} = \frac{C(s)P(s)}{1 + C(s)P(s)} = \frac{H}{sL_m + H} \tag{5}$$

Impedance reshaping control obtains harmonic current instructions based on harmonic voltage calculation and it can be externally equivalent to the virtual impedance $Z_a$ at harmonic frequency. Impedance $Z_a$ consists of inductance component $L_a$ and resistance component $R_a$.

$$Z_a = \frac{ku_h}{i_h/k} = \frac{k^2}{G} + s\frac{k^2 L_m}{GH} = R_a + sL_a \tag{6}$$

As shown in Fig. 6, to facilitate the analysis, the line impedance is equivalent to the parallel form of the traction network equivalent inductance $L_n$ and equivalent capacitance $C_n$. When the network voltage resonance occurs, it can be considered as a parallel resonance of equivalent inductance and equivalent capacitance of traction network. The impedance reshaping control link of the train auxiliary converter is equivalent to the parallel equivalent impedance $Z_a$ at the location of the train. $Z$ is the impedance value of the position where the train access to traction network. At this point, the impedance value $Z$ corresponding to this position will change.

The line impedance $Z_n$ is determined as follows:

$$Z_n = \frac{(sL_n) \times \frac{1}{(sC_n)}}{(sL_n) + 1/(sC_n)} = \frac{(sL_n)}{(L_nC_n)s^2 + 1} \tag{7}$$

After the impedance reshaping control of the auxiliary converter, the new impedance of the train location is as shown in (8).

$$Z = \frac{Z_n \times Z_a}{Z_n + Z_a} = \frac{(k^2L_nL_m)s^2 + (k^2HL_n)s}{(k^2L_nL_mC_n)s^3 + (k^2HL_nC_n)s^2 + (HGL_n + k^2L_m)s + k^2H} \tag{8}$$

In the absence of equivalent impedance $Z_a$, $Z$ is the line impedance $Z_n$, thus the original characteristic frequency of $Z$ is:

$$\omega_o = \frac{1}{\sqrt{L_nC_n}} \tag{9}$$

By adding the impedance reshaping control, and ignoring the influence of resistance on characteristic frequency, the new characteristic frequency of Z is approximated.

$$\omega_m \approx \sqrt{(L_n + L_a)/L_aL_nC_n} \tag{10}$$

$$\frac{\omega_m}{\omega_o} \approx \sqrt{\frac{L_n + L_a}{L_a}} = \sqrt{1 + \frac{L_n}{L_a}} \tag{11}$$

When the impedance reshaping control is added, the characteristic frequency becomes larger, and the equivalent impedance is smaller.

The impedance $Z$ is paralleled by the line impedance $Z_n$ and train equivalent impedance $Z_a$, and the value of $Z$ is less than each of the two values. Provided that the $Z_a$ is sufficiently small, the $Z$ can be ensured to be small enough to suppress the voltage resonance at this point. Therefore, this method can adapt to the situation of train movement and the variation of traction network parameters. If the train equivalent impedance is controlled, the change of external conditions will not affect the suppression effect.

Equivalent impedance value at original characteristic frequency:

$$Z_{a/\omega=\omega_o} = R_a + sL_a = R_a + j\frac{L_a}{\sqrt{L_nC_n}} = \frac{k^2}{G} + j\frac{k^2L_m}{GH\sqrt{L_nC_n}} \tag{12}$$

The impedance value at the characteristic frequency is approximately:

$$Z_{/\omega=\omega_m} = \frac{(L_n + \frac{k^2L_m}{GH})\frac{L_m}{H}}{L_nC_n} - j\sqrt{\frac{(L_n + \frac{k^2L_m}{GH})\frac{k^2L_m}{GH}}{L_nC_n}} \tag{13}$$

$$\left|Z_{/\omega=\omega_m}\right| \le \left|Z_{a/\omega=\omega_m}\right| = \left|\frac{k^2}{G} + j\frac{k^2L_m\sqrt{1 + \frac{L_n}{L_a}}}{GH\sqrt{L_nC_n}}\right| \tag{14}$$

**TABLE 1. Harmonic current distortion limit ($I_{hn}/I_L$ * 100%).**

| Frequency | 3≤n<11 | 11≤n<17 | 17≤n<23 | 23≤h<35 | 35≤h≤50 | THD |
|---|---|---|---|---|---|---|
| Limit | 4.0 | 2.0 | 1.5 | 0.6 | 0.3 | 5.0 |

$I_{hn}$ is n-th harmonic current, $I_L$ is fundamental current.

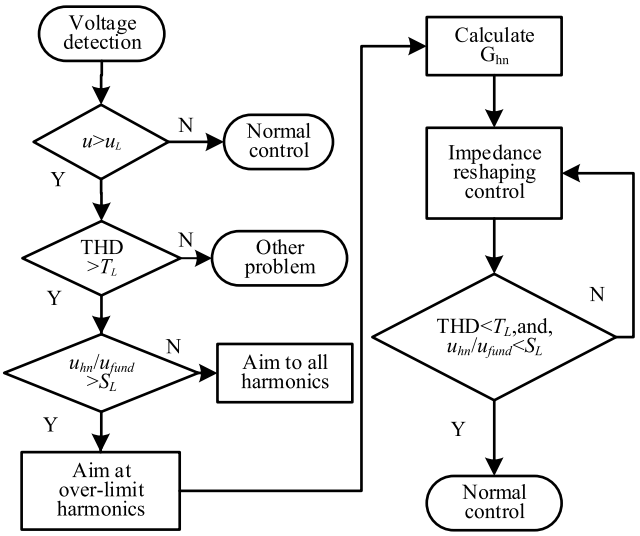


**FIGURE 7. Suppression strategy of impedance reshaping control for auxiliary converter.**

The characteristic frequency and corresponding impedance value are related to the line parameters and train parameters.

According to the harmonic voltage limit value and harmonic current source value, we determine the impedance limits within a certain range. Under normal circumstances, the harmonic current source value cannot exceed harmonic current limited value. The limiting value of the harmonic voltage is fixed. The limiting range of impedance value can be obtained. In the case of line parameters and harmonic frequency changes, if the control is appropriate, it can effectively suppress resonance.

### B. SUPPRESSION STRATEGY OF IMPEDANCE RESHAPING CONTROL FOR THE AUXILIARY CONVERTER

According to the IEEE standard 519-2014 [30], the single harmonic voltage distortion is less than 3%, and the total voltage distortion is less than 5%. And the specific harmonic current limit is shown in Table 1. For the harmonic current, the frequency is different, as is the corresponding harmonic limit. In the corresponding harmonic range, the corresponding Z and G are calculated respectively.

After voltage detection, it is necessary to determine whether the system is normal or unstable. Once the resonance occurs, the impedance reshaping control starts and keeps running. Inspecting the system status, if the system restores stability, normal control re-uses. With several each resonance frequencies, the suppression strategy of impedance reshaping

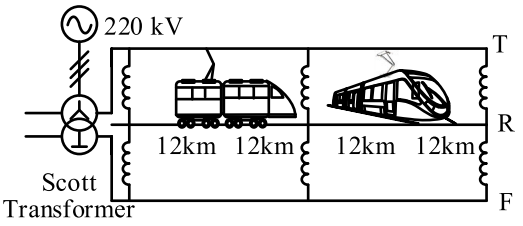


**FIGURE 8.** Circuit topology in an example.

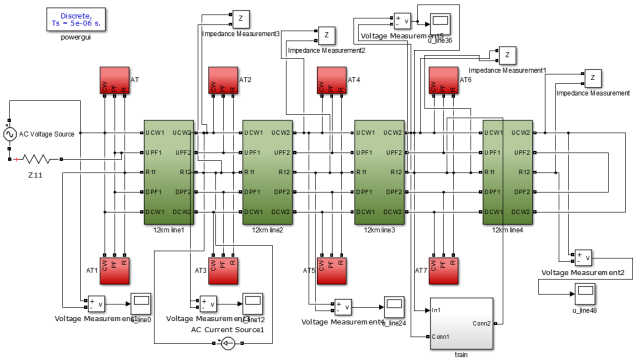

**FIGURE 9.** Diagram of Simulink model.

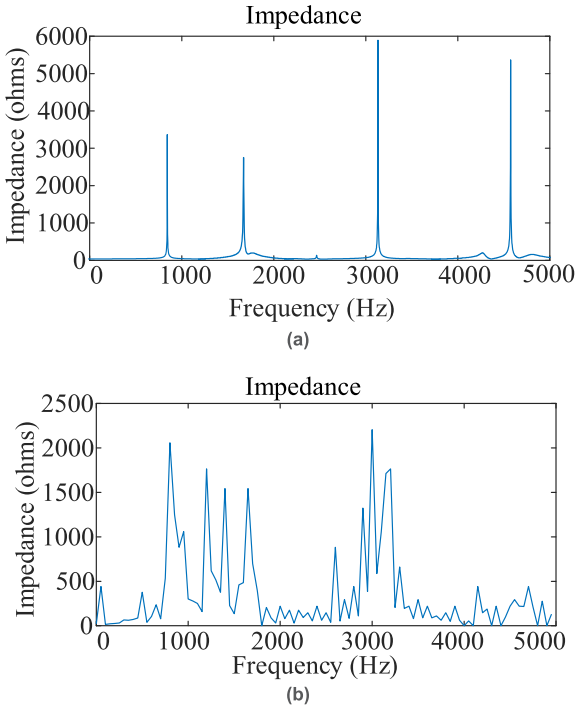


**FIGURE 10.** Comparison of theoretical impedance and simulated system impedance. (a) Impedance of the circuit in Fig. 6. (b) Impedance of the simulated system.

control for auxiliary converter is shown in Fig. 7. u is the instantaneous value of grid-side voltage; $u_L$ is the limit value of grid-side voltage, which in the subsequent discussion is defined as 43 kV; $T_L$ is the limit value of total harmonic distortion rate; $u_{hn}$ is n-th harmonic component of grid-side voltage; $u_{fund}$ is the fundamental component of the grid-side voltage; and $S_L$ is the limit value of single harmonic distortion rate which can be found in Table 1. $G_{hn}$ is the control parameter $G$ corresponding to the n-th harmonic component.

In the strategy, we calculate $G_{hn}$ with different frequencies.

$$i_{hn} \times Z_{hn} = u_{hn} \leq 27.5 \times 10^3 \times 3\% \tag{15}$$

$$i_{hn} < i_{h\text{limit}} \tag{16}$$

$$Z_{hn} \leq u_{hn}/i_{hn} \tag{17}$$

$$|Z_{hn}| < |Z_a| = \left|\frac{k^2}{G} + j\omega\frac{k^2 L_m}{GH}\right| \tag{18}$$

$L_m$, $k$ and $H$ are known.

$$G_{hn} > \left|\frac{k^2(H + j\omega L_m) \times i_{hn}}{H \times u_{hn}}\right| \tag{19}$$

## IV. SIMULATION RESULTS

Resistive active power filter (RAPF) is an effective approach to mitigate harmonics [25], [26]. The train impedance reshaping method proposed in this paper is similar to RAPF method in principle and both can achieve the effect of harmonic suppression. The RAPF method requires additional power circuit of the active filter power converters to be installed on lines. Adding additional hardware equipment to each section of the line will result in high cost. It can only suppress specific harmonics in most cases, such as 5th or 7th harmonics, due to the limitations of fixed circuits and switching devices. The installation position of the equipment on the line will also have an impact on the suppression effect. Our proposed train impedance reshaping method uses train auxiliary converter as the main circuit to suppress harmonics. In this way, there is no additional hardware cost, and the suppression effect is not affected by the location. Because of the use of SiC devices, the detected harmonics can be suppressed effectively in a wide frequency range.

In this section, the model of traction network and train is established using Simulink. The trains-network system is divided into three parts: the traction network, the left train as harmonic source, and the right train which is controllable.

**TABLE 2.** Simulation parameters of the train.

| Winding | Primary side | Traction | Auxiliary |
|---|---|---|---|
| Winding nominal power (kVA) | 7051 | 6400 | 2×217 |
| Winding nominal voltage (V) | 25k | 4×1950 | 2×304 |
| Winding nominal current (A) | 282 | 4×820 | 2×714 |
| AC side inductance(H) | | | 88 μ |
| DC side supporting capacitance(F) | | | 32 m |
| switching frequency (Hz) | | | 5 k |

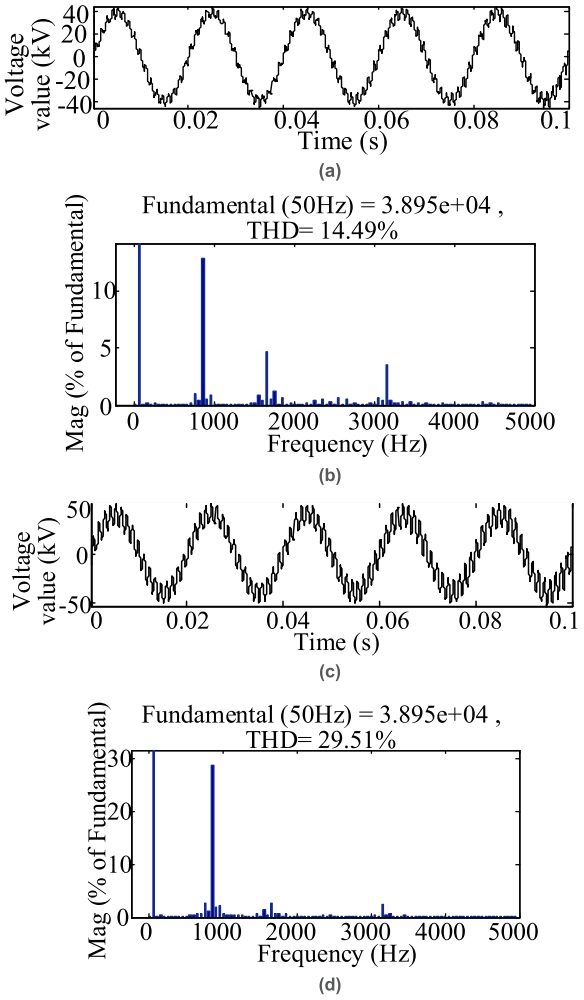


**FIGURE 11.** Voltage waveform and FFT analysis when resonance happens. (a) Voltage waveform at 12 km. (b) FFT analysis at 12 km. (c) Voltage waveform at 36km. (d) FFT analysis at 36 km.

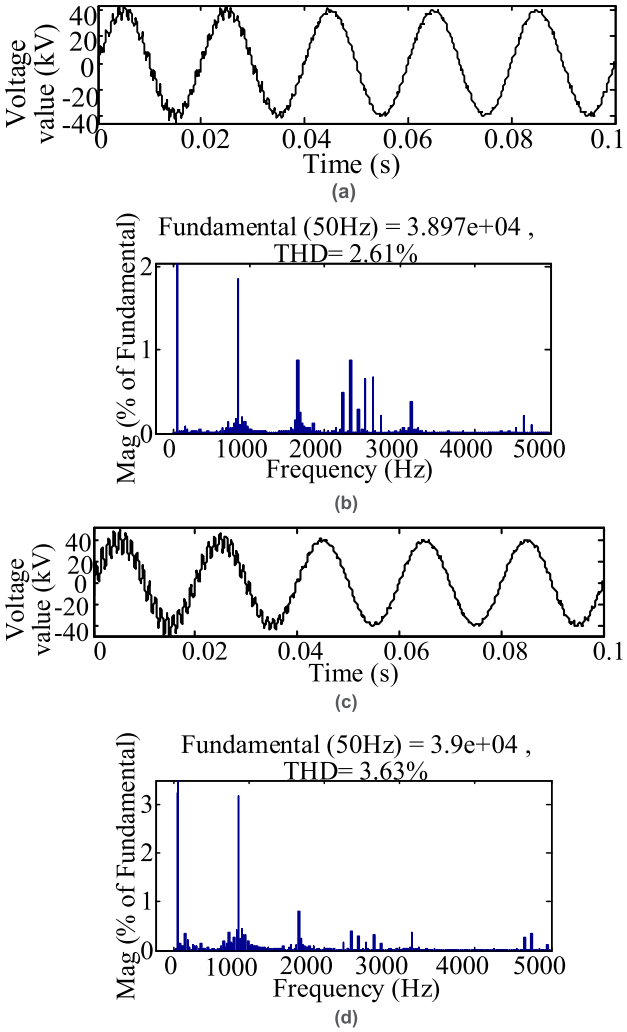


**FIGURE 12.** Voltage waveform and FFT analysis when resonance is suppressed. (a) Voltage waveform at 12 km. (b) FFT analysis at 12 km. (c) Voltage waveform at 36km. (d) FFT analysis at 36 km.

The line simulation parameters are designed according to a line in China. The length of the power supply arm is 48 km. The harmonic source is at 12 km, and the controllable train is at 36 km, as shown in Fig. 8. The simulation parameters referring to actual operation parameters of the train are shown in Table 2. The left train is simplified as a harmonic source. The line has characteristic impedance at 850Hz. The current loop control parameter, H, is set to 1.

The simulation model with specific parameters is shown in Fig. 9. As shown in Fig. 10, by comparing the theoretical impedance and the simulated system impedance, it is proved that the adequacy of simulation results.

As shown in Fig. 11, the peak amplitudes of the resonance voltages are over 40 kV at 12km and around 50 kV at 36km, the total distortion rate of the voltages are 14.49% at 12km and 29.51% at 36km, and the harmonics are mainly in the three frequencies of 850Hz, 1650Hz and 3050Hz. We then calculate G using these three frequencies respectively. 850Hz is the most obvious resonant frequency. The harmonic distortion rate of this frequency exceeds 10% and near 30% at 12km and 36km. This shows that the resonance does not only occur at the location of the harmonic source. Therefore, it is necessary to consider the resonance caused by other harmonic sources.

As shown in Fig. 12, the peak value of the voltage waveform decreases obviously, the amplitude returns to around 40 kV. The total harmonic distortion rate of the voltage drops from 14.49% to 2.61% at 12 km and from 29.51% to 3.63% at 36 km. The harmonic distortion rate of 850Hz decreases to around 3% at 36km. The harmonic content of other resonant frequencies is also significantly reduced.

The resonance phenomenon is suppressed effectively, and the power quality is significantly improved. Simulation results validates the effectiveness of the suppression strategy.

## V. EXPERIMENTAL RESULTS

The suppression strategy is tested using the small power experimental platform. Its photos are shown in Fig. 13 and its circuit diagram is shown in Fig. 14.

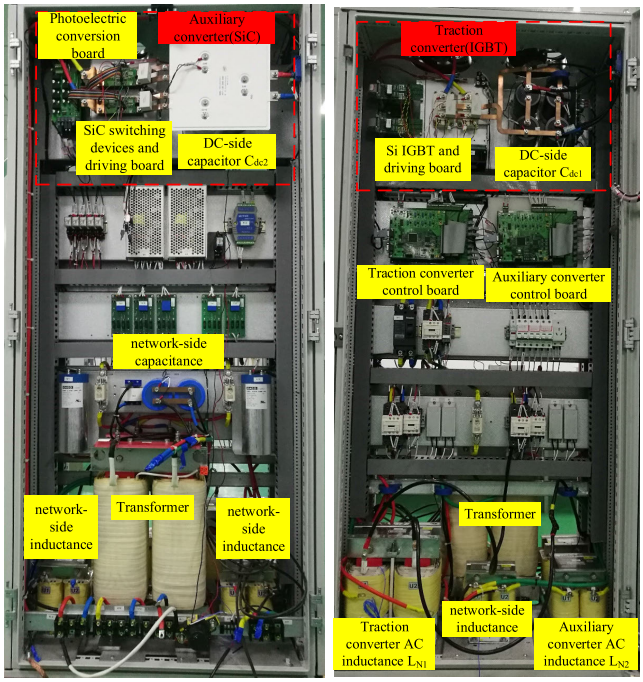


**FIGURE 13.** Photos of the small power experimental platform.

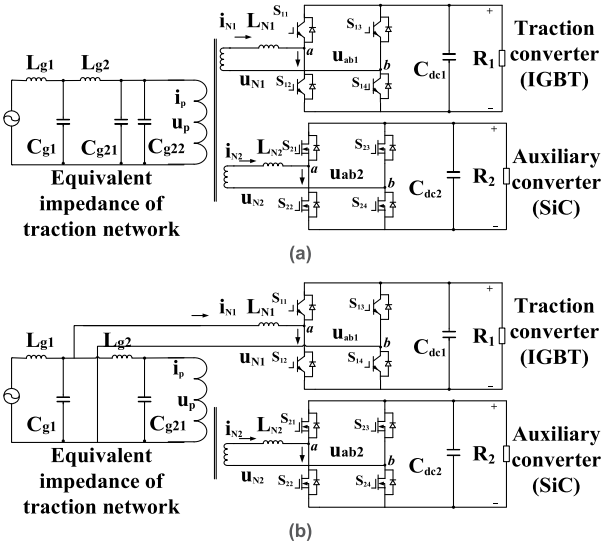


**FIGURE 14.** Circuit diagram of the small power experimental platform with different connections. (a) Resonance generated by the harmonic current of the train itself. (b) Resonance generated by the harmonic current of other trains.

### A. THE SMALL POWER EXPERIMENTAL PLATFORM

As shown in Fig. 14, the hardware in the small power experimental platform is composed of three parts: network-side impedance circuit used to simulate traction network, traction converter and SiC auxiliary converter. Parameters of them are shown in Table 3. Different topologies are used in experiments. Different resonance frequency can be tested with different circuit combination.

In Fig. 14 (a), both traction converter and auxiliary converter are on the same side of transformer. This is used to simulate the resonance generated by the harmonics of the train itself. The traction converter uses normal control mode. As a harmonic source, traction converter changes the frequency distribution of harmonics by changing its switching frequency. In Fig. 14 (b), traction transformer and auxiliary transformer are not in the same position. The traction converter represents other trains that generate harmonics. The auxiliary converter using impedance reshaping control

**TABLE 3.** Parameters of the power experimental platform.

| Items | Value |
|---|---|
| network-side inductance $Lg_1$ | 2.46mH |
| network-side capacitance $Cg_1$ | 0.5uF |
| network-side inductance $Lg_2$ | 0.5mH |
| network-side capacitance $Cg_{21}$, $Cg_{21}$ | 35μF, 35μF |
| traction converter AC inductance $L_{N1}$ | 7mH |
| traction converter load $R_1$ | 10 Ω |
| auxiliary converter AC inductance $L_{N2}$ | 1.25 mH |
| auxiliary converter load $R_2$ | 25.6 Ω |
| traction converter switching frequency | 600, 2.15k |
| auxiliary converter switching frequency | 20k |
| Transformer ratio | 380:300:200 |

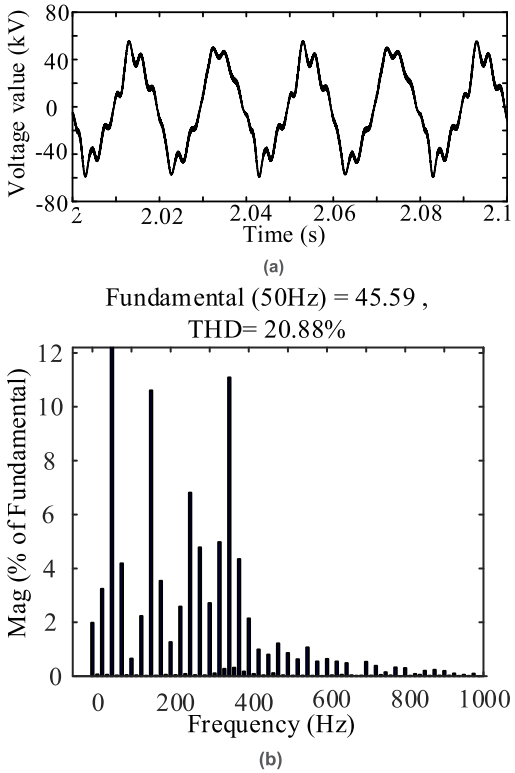


**FIGURE 15.** The experimental results with harmonic current of the train itself, 350Hz resonance when SiC converter is normally controlled. (a) Primary voltage, $u_p$, waveform. (b) Primary voltage, $u_p$, FFT.

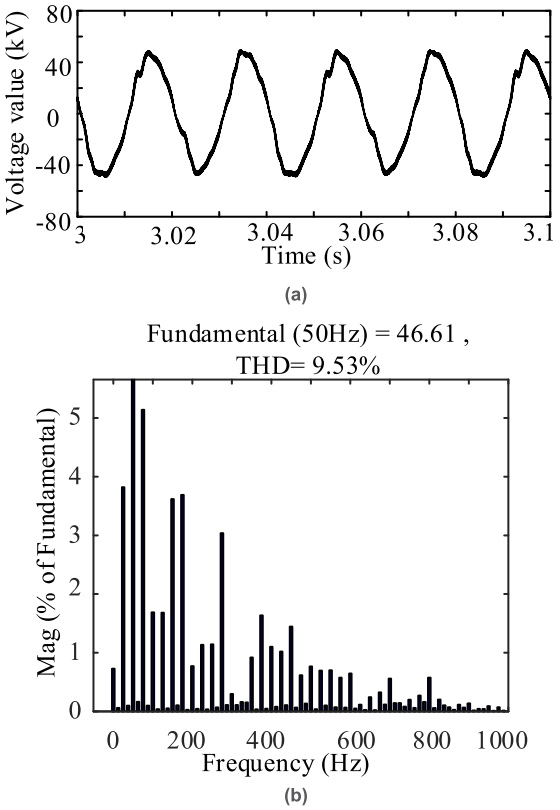


**FIGURE 16.** The experimental results with harmonic current of the train itself, when SiC converter is with impedance reshaping controlled. (a) Primary voltage, $u_p$, waveform. (b) Primary voltage, $u_p$, FFT.

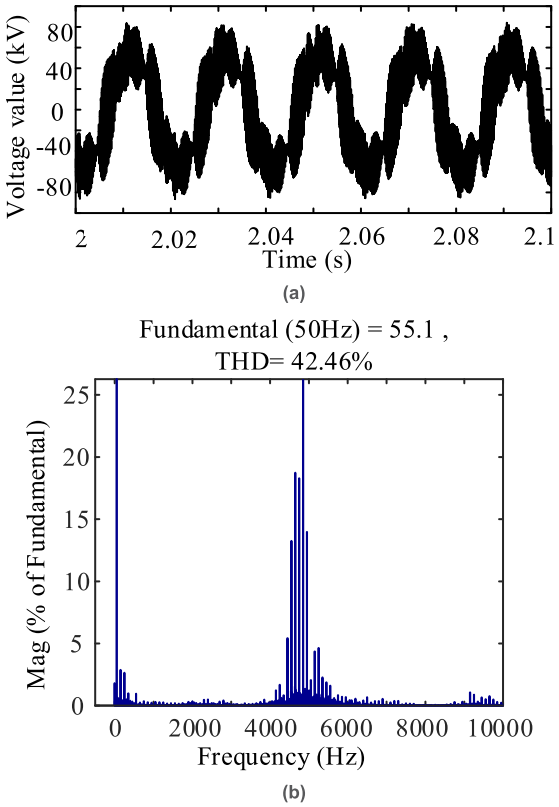


**FIGURE 17.** The experimental results with harmonic current of the train itself, 4850Hz resonance when SiC converter is normally controlled. (a) Primary voltage, $u_p$, waveform. (b) Primary voltage, $u_p$, FFT.

for resonance suppression represents the train we need to control.

### B. EXPERIMENTAL RESULTS OF THE SMALL POWER EXPERIMENTAL PLATFORM

With $Lg_1$, $Cg_1$, $Lg_2$, $Cg_{21}$ and $Cg_{22}$, as shown in Fig. 14(a), the resonance frequency of the voltage at the primary side of the train is around 350Hz. As shown in Fig. 15, the primary voltage THD is 20.88%, 350Hz voltage harmonic content is 11.77%, and 350Hz current harmonic content is 12.19%. SiC-side 350Hz impedance value is 6.78, equivalent to the primary side of the transformer is 24.48.

In the SiC impedance reshaping control, the virtual impedance value is set to 2. As shown in Fig. 16, the peak value of the voltage waveform decreases from above 60V to around 50V. The primary voltage THD is 9.53%, 350Hz voltage harmonic content is 0.66%, and 350Hz current harmonic content is 3.74%. SiC-side 350Hz impedance value is 1.26, equivalent to the primary side of the transformer is 4.55. The actual impedance value is less than the set value. It fits the theoretical analysis. The suppression effect is also obvious.

Changing to network to only Lg1 and Cg1, the SiC converter and IGBT converter operate separately with switching frequency 20 kHz and 2.35 kHz. As shown in Fig. 17, the resonant frequency 4850 Hz, and the corresponding primary voltage harmonic content is 28.46%, corresponding primary current harmonic content is 0.4035% at this frequency. Impedance value is 443 at the transformer primary side at 4850Hz.

In the SiC impedance reshaping control, the virtual impedance value is set to 52. As shown in Fig. 18, with impedance reshaping control, impedance value is 106 at 4850Hz. With the increase of harmonic frequency, the impedance reshaping effect is weakened, but impedance still decrease. Primary voltage THD is also decreased to 12.07%. The peak voltage is reduced from above 80V to around 60 V, and the effect is still remarkable.

With Lg1, Cg1, Lg2, and Cg21, as shown in Fig. 14(b), the resonance frequency of the voltage at the primary side of the train is around 550Hz. As shown in Fig. 19, the voltage THD is 21.81%, 550Hz voltage harmonic content is 14.01%. And 550Hz current harmonic content is 7.767%. SiC-side 550Hz impedance value is 12.55, equivalent to the primary side of the transformer is 45.3.

In the SiC impedance reshaping control, the virtual impedance value is set to 5. As shown in Fig. 20, the peak value of the SiC voltage waveform decreases from above 40V to around 32V. The voltage THD is 10.28%, 550Hz voltage harmonic content is 5.477%. And 550Hz current harmonic content is 6.835%. SiC-side 550Hz impedance value is 5.25, equivalent to the primary side of the transformer is 18.95.

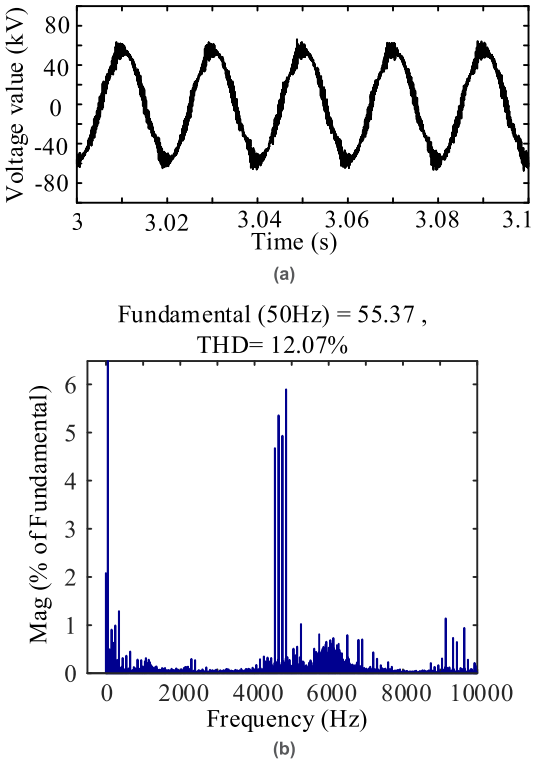


**FIGURE 18.** The experimental results with harmonic current of the train itself, when SiC converter is with impedance reshaping controlled. (a) Primary voltage, $u_p$, waveform. (b) Primary voltage, $u_p$, FFT.

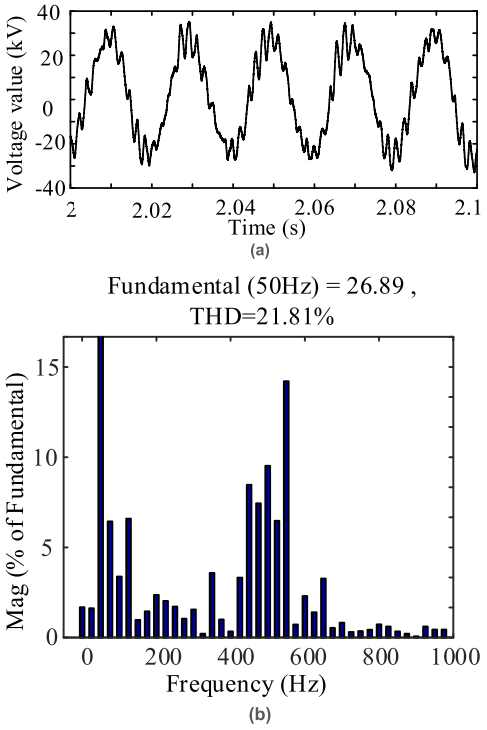


**FIGURE 19.** The experimental results with harmonic current of the other train, 550Hz resonance when SiC converter is normally controlled. (a) SiC APU AC-voltage, $u_{N2}$, waveform. (b) SiC APU AC-voltage, $u_{N2}$, FFT.

The actual impedance value is close to the set value. It fits the theoretical analysis. The suppression effect is also obvious.

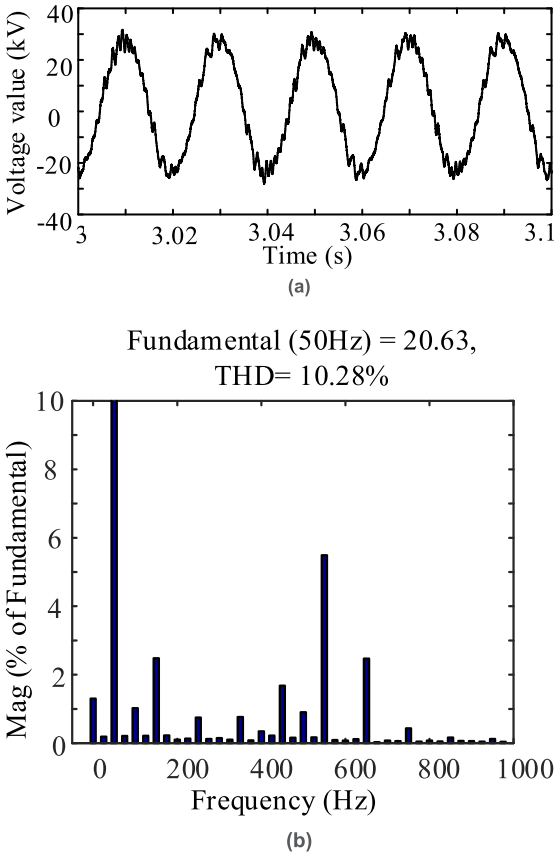


**FIGURE 20.** The experimental results with harmonic current of the other train, when SiC converter is with impedance reshaping controlled. (a) SiC APU AC-voltage, $u_{N2}$, waveform. (b) SiC APU AC-voltage, $u_{N2}$, FFT.

Summary and comparison of experimental results are shown in Table 4.

Circuit I is the circuit shown in Figure 14(a). Circuit II is the circuit shown in Figure 14(a), but without $Lg_2$, $Cg_{21}$ and $Cg_{22}$. Circuit III is the circuit shown in Figure 14(b). In all cases, after the resonance suppression strategy is put in, the equivalent harmonic impedance approaches the set value, voltage amplitude decreases, and waveform improves significantly. In Circuit I and Circuit II, both traction converter and auxiliary converter are on the same side of transformer to simulate one train. Different frequency can be tested by different network-side circuit combination. The comparison between the two cases shows that the resonance suppression effect is obvious at both low and high frequencies. In Circuit III, the position of traction converter is changed to simulate another train which is in the different locations of traction network. Comparing the experimental results of Circuit I and Circuit III, it shows that the proposed suppression method is effective whether the resonance is caused by the train itself or other trains on the same traction network. The above experimental results show that the proposed harmonic resonance suppression strategy is effective in different circuit topologies, with different harmonic sources and at different resonant frequencies.

**TABLE 4. Summary and comparison of experimental results.**

| Different circuits | Circuit I | Circuit II | Circuit III |
|---|---|---|---|
| Corresponding figures | Fig. 15 and 16 | Fig. 17 and 18 | Fig. 19 and. 20 |
| Harmonic source | the train itself | the train itself | other trains |
| Resonant frequency | 350Hz | 4850Hz | 550Hz |
| Primary voltage THD changes (before and after suppression) | 20.88% to 9.53% | 42.26% to 12.07% | 21.81% to 10.28% |
| Voltage harmonic content changes at resonance frequency (before and after suppression) | 11.77% to 0.66% | 28.46% to 5.86% | 14.01% to 5.477% |
| Equivalent harmonic impedance changes at resonant frequency (before and after suppression) | 24.48 to 4.55 | 443 to 91.22 | 45.3 to 18.95 |

## VI. CONCLUSION

In this paper, a harmonic resonance suppression strategy of the trains-network system based on impedance reshaping by auxiliary converter of electrical locomotive is proposed. Based on the analysis of harmonics resonances mechanism of the trains-network systems, the harmonic impedance of the train is reshaped to reduce the equivalent harmonic impedance of the train position. The resonance formation condition is broken, and resonances are suppressed. After applying this suppression method, the voltage amplitude of the train entering the traction network is shown to have obviously decreased, the total distortion rate is significantly reduced, the sine degree of the waveform is significantly improved, and the suppression effect is achieved.

The trains-network system harmonic resonance suppression based on the impedance reshaping control of the auxiliary converter proposed in this paper can effectively restrain the harmonic resonance of trains without adding system hardware and has little impact on the function of the system itself. And this strategy can suppress harmonic resonance even if the train is moving and the impedance is changing. This strategy is valid whether the resonance is caused by the train itself or other trains on the same traction network. Due to the application of SiC devices, the frequency range of effective suppression is very wide, reaching about 5000Hz. It is not only effective for multiples of 50Hz, but also for non-multiples. The proposed strategy is cost-effective, efficient, and unaffected by external conditions.

## ACKNOWLEDGMENT

The authors would like to thank Toshiba Infrastructure Systems & Solutions Corporation for providing support.

## REFERENCES

[1] E. Mollerstedt and B. Bernhardsson, "Out of control because of harmonics-an analysis of the harmonic response of an inverter locomotive," *IEEE Control Syst. Mag.*, vol. 20, no. 4, pp. 70–81, Aug. 2000, doi: 10.1109/37.856180.

[2] H. Lee, C. Lee, G. Jang, and S.-H. Kwon, "Harmonic analysis of the Korean high-speed railway using the eight-port representation model," *IEEE Trans. Power Del.*, vol. 21, no. 2, pp. 979–986, Apr. 2006, doi: 10.1109/TPWRD.2006.870985.

[3] Z. He, H. Hu, Y. Zhang, and S. Gao, "Harmonic resonance assessment to traction power-supply system considering train model in China high-speed railway," *IEEE Trans. Power Del.*, vol. 29, no. 4, pp. 1735–1743, Aug. 2014, doi: 10.1109/TPWRD.2013.2284233.

[4] M. Brenna, F. Foiadelli, and D. Zaninelli, "Electromagnetic model of high speed railway lines for power quality studies," *IEEE Trans. Power Electron.*, vol. 25, no. 3, pp. 1301–1308, Aug. 2010, doi: 10.1109/TPWRS.2010.2042979.

[5] H. Hu, H. Tao, F. Blaabjerg, X. Wang, Z. He, and S. Gao, "Train–network interactions and stability evaluation in high-speed railways–Part I: Phenomena and modeling," *IEEE Trans. Power Electron.*, vol. 33, no. 6, pp. 4627–4642, Jun. 2018, doi: 10.1109/TPEL.2017.2781880.

[6] H. Hu, H. Tao, and X. Wang, "Train–network interactions and stability evaluation in high-speed railways—Part II: Influential factors and verifications," *IEEE Trans. Power Electron.*, vol. 33, no. 6, pp. 4643–4659, Jun. 2018, doi: 10.1109/TPEL.2017.2781879.

[7] S. Kejian, W. Mingli, and V. G. Agelidis, "Line current harmonics of three-level neutral-point-clamped electric multiple unit rectifiers: Analysis, simulation and testing," *IET Power Electron.*, vol. 7, no. 7, pp. 1850–1858, Jul. 2014, doi: 10.1049/iet-pel.2013.0683.

[8] X. Wang, F. Blaabjerg, and W. Wu, "Modeling and analysis of harmonic stability in an AC power-electronics-based power system," *IEEE Trans. Power Electron.*, vol. 29, no. 12, pp. 6421–6432, Dec. 2014, doi: 10.1109/TPEL.2014.2306432.

[9] X. Wang, L. Harnefors, and F. Blaabjerg, "Unified impedance model of grid-connected voltage-source converters," *IEEE Trans. Power Electron.*, vol. 33, no. 2, pp. 1775–1787, Feb. 2018, doi: 10.1109/TPEL.2017.2684906.

[10] Y. Wang, X. Wang, F. Blaabjerg, and Z. Chen, "Harmonic instability assessment using state-space modeling and participation analysis in inverter-fed power systems," *IEEE Trans. Ind. Electron.*, vol. 64, no. 1, pp. 806–816, Jan. 2017, doi: 10.1109/TIE.2016.2588458.

[11] K. Song, G. Konstantinou, W. Mingli, P. Acuna, R. P. Aguilera, and V. G. Agelidis, "Windowed SHE-PWM of interleaved four-quadrant converters for resonance suppression in traction power supply systems," *IEEE Trans. Power Electron.*, vol. 32, no. 10, pp. 7870–7881, Oct. 2017, doi: 10.1109/TPEL.2016.2636882.

[12] K. Zhou, Z. Qiu, N. R. Watson, and Y. Liu, "Mechanism and elimination of harmonic current injection from single-phase grid-connected PWM converters," *IET Power Electron.*, vol. 6, no. 1, pp. 88–95, Jan. 2013, doi: 10.1049/iet-pel.2012.0291.

[13] H. Cui, W. Song, H. Fang, X. Ge, and X. Feng, "Resonant harmonic elimination pulse width modulation-based high-frequency resonance suppression of high-speed railways," *IET Power Electron.*, vol. 8, no. 5, pp. 735–742, May 2015, doi: 10.1049/iet-pel.2014.0204.

[14] L. Wang, X. Han, C. Ren, Y. Yang, and P. Wang, "A modified one-cycle-control-based active power filter for harmonic compensation," *IEEE Trans. Ind. Electron.*, vol. 65, no. 1, pp. 738–748, Jan. 2018, doi: 10.1109/TIE.2017.2682021.

[15] W. R. N. Santos, E. R. C. D. Silva, and C. B. Jacobina, "The transformerless single-phase universal active power filter for harmonic and reactive power compensation," *IEEE Trans. Power Electron*, vol. 29, no. 7, pp. 3563–3572, Jul. 2014, doi: 10.1109/TPEL.2013.2280691.

[16] D. Pan, X. Ruan, C. Bao, W. Li, and X. Wang, "Capacitor-current-feedback active damping with reduced computation delay for improving robustness of LCL-type grid-connected inverter," *IEEE Trans. Power Electron.*, vol. 29, no. 7, pp. 3414–3427, Jul. 2014, doi: 10.1109/TPEL.2013.2279206.

[17] X. Li, X. Wu, Y. Geng, X. Yuan, C. Xia, and X. Zhang, "Wide damping region for LCL-type grid-connected inverter with an improved capacitor-current-feedback method," *IEEE Trans. Power Electron.*, vol. 30, no. 9, pp. 5247–5259, Sep. 2015, doi: 10.1109/TPEL.2014.2364897.

[18] X. Wang, F. Blaabjerg, and P. C. Loh, "Virtual RC damping of LCL-filtered voltage source converters with extended selective harmonic compensation," *IEEE Trans. Power Electron.*, vol. 30, no. 9, pp. 4726–4737, Sep. 2015, doi: 10.1109/TPEL.2014.2361853.

[19] X. Wang, F. Blaabjerg, M. Liserre, Z. Chen, J. He, and Y. Li, "An active damper for stabilizing power-electronics-based AC systems," *IEEE Trans. Power Electron.*, vol. 29, no. 7, pp. 3318–3329, Jul. 2014, doi: 10.1109/TPEL.2013.2278716.

[20] M. Hanif, V. Khadkikar, and W. Xiao, "Two degrees of freedom active damping technique for LCL filter-based grid connected PV systems," *IEEE Trans. Ind. Electron.*, vol. 61, no. 6, pp. 2795–2803, Jun. 2014, doi: 10.1109/TIE.2013.2274416.

[21] J. Xu, S. Xie, and T. Tang, "Active damping-based control for grid-connected LCL-filtered inverter with injected grid current feedback only," *IEEE Trans. Ind. Electron.*, vol. 61, no. 9, pp. 4746–4758, Sep. 2014, doi: 10.1109/TIE.2013.2290771.

[22] X. Wang, F. Blaabjerg, and P. C. Loh, "Grid-current-feedback active damping for LCL resonance in grid-connected voltage-source converters," *IEEE Trans. Power Electron.*, vol. 31, no. 1, pp. 213–223, Jan. 2016, doi: 10.1109/TPEL.2015.2411851.

[23] J. He, Y. W. Li, D. Bosnjak, and B. Harris, "Investigation and active damping of multiple resonances in a parallel-inverter-based microgrid," *IEEE Trans. Power Electron.*, vol. 28, no. 1, pp. 234–246, Jan. 2013, doi: 10.1109/TPEL.2012.2195032.

[24] Y. Li, F. Liu, and T. K. Saha, "Hybrid inductive and active filtering method for damping harmonic resonance in distribution network with non-linear loads," *IET Power Electron.*, vol. 8, no. 9, pp. 1616–1624, Sep. 2015, doi: 10.1049/iet-pel.2014.0521.

[25] X. Sun, R. Han, and H. Shen, "A double-resistive active power filter system to attenuate harmonic voltages of a radial power distribution feeder," *IEEE Trans. Power Electron.*, vol. 31, no. 9, pp. 6203–6216, Sep. 2016, doi: 10.1109/TPEL.2015.2500913.

[26] X. Sun, J. Zeng, and Z. Chen, "Site selection strategy of single-frequency tuned R-APF for background harmonic voltage damping in power systems," *IEEE Trans. Power Electron.*, vol. 28, no. 1, pp. 135–143, Jan. 2013, doi: 10.1109/TPEL.2011.2179121.

[27] S. Liu, Z. Yang, F. Lin, Q. Lian, W. Shi, and H. Sun, "Medium-frequency oscillation analysis in high-speed railway system considering power supply system with LCL model," in *Proc. 42nd Annu. Conf. IEEE Ind. Electron. Soc.*, Florence, Italy, Oct. 2016, pp. 3470–3475.

[28] C. Chen and Y. Chen, "Application of adaptive model-based scheme for harmonic diagnosis and compensation of grid-connected converters," *IEEE Trans. Ind. Electron.*, vol. 65, no. 1, pp. 770–777, Jan. 2018, doi: 10.1109/TIE.2017.2677322.

[29] L. Feng, W. Yao, and Y. Wang, "A novel DFT algorithm used in active power filter under frequency distortion," in *Proc. IEEE 3rd Int. Future Energy Electron. Conf. ECCE Asia*, Kaohsiung, Taiwan, Jun. 2017, pp. 1375–1379.

[30] *IEEE Recommended Practice and Requirements for Harmonic Control in Electric Power Systems*, IEEE Standard 519-2014 (Revision IEEE Standard 519-1992), Jun. 2014, pp. 1–29.

**SHIHUI LIU** (S'15) received the B.S. degree in electrical engineering from Beijing Jiaotong University, Beijing, China, in 2014. She is currently pursuing the Ph.D. degree with the School of Electrical Engineering, Beijing Jiaotong University.

Her current research interests include the areas of electric traction systems for rail vehicles, vehicle-power supply network coupling system, and power quality.

Ms. Liu was a recipient of the Best Session Presentation during the 42nd Annual Conference of the IEEE Industrial Society (IEEE-IECON2016), in 2016.

**FEI LIN** (M'05) received the B.S. degree from Xi'an Jiaotong University, Xi'an, China, the M.S. degree from Shandong University, Jinan, China, and the Ph.D. degree from Tsinghua University, Beijing, China, in 1997, 2000, and 2004, respectively, all in electrical engineering.

He is currently a Professor with the School of Electrical Engineering, Beijing Jiaotong University. His research interests include traction converter and motor drives, energy management for railway systems, and digital control of power-electronic-based devices.

**XIAOCHUN FANG** (S'14–M'17) received the B.S. and Ph.D. degrees from Beijing Jiaotong University, Beijing China, in 2010 and 2016, respectively, both in engineering.

He is currently a Lecturer with the School of Electrical Engineering, Beijing Jiaotong University, Beijing. His research interests include traction converter and motor drives, energy management for railway systems, IGBT fault mechanism, and failure prediction.

**ZHONGPING YANG** (M'14) received the B.Eng. degree from the Tokyo University of Mercantile Marine, Tokyo, Japan, in 1997, and the M.Eng. and Ph.D. degrees from the University of Tokyo, Tokyo, in 1999 and 2002, respectively, all in electrical engineering.

He is currently a Professor with the School of Electrical Engineering, Beijing Jiaotong University. His research interests include high-speed rail integration technology, traction and regenerative braking technology, and wireless power transfer of urban rail vehicles.

**ZHIWEI ZHANG** (M'18) received the Ph.D. degree in electrical engineering from the Huazhong University of Science and Technology, Wuhan, China, in 2016.

He is currently a Visiting Scholar with the Department of Electrical and Computer Engineering, The Ohio State University, Columbus, OH, USA. His major research interests include the design and analysis of high-performance electric machines, variable-speed AC drives, and transportation electrification.